ChemComm

Accepted Manuscript

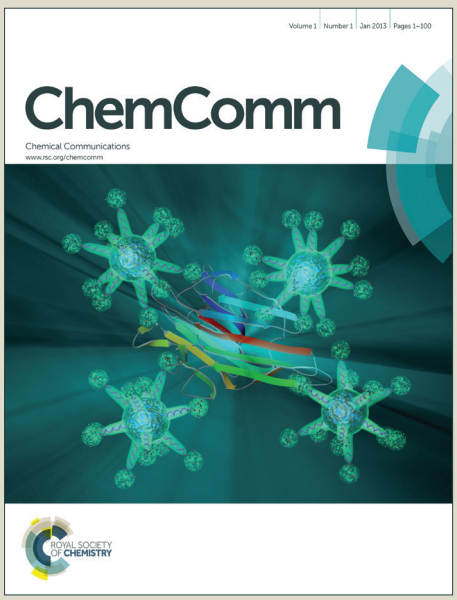

ROYAL SOCIETY OF CHEMISTRY

www.rsc.org/chemcomm

A table of contents

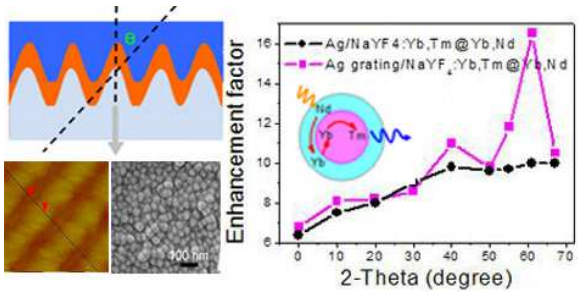

The UCL enhancement of $NaYF_4:Yb^{3+},Tm^{3+}@NaYF_4:Yb^{3+},Nd^{3+}$ core-shell NCs resulting from Ag grating structure provides a novel insight of improving UCL.

Cite this: DOI: 10.1039/c0xx00000x

www.rsc.org/xxxxxx

ARTICLE TYPE

Upconversion Luminescence Enhancement of Yb^{3+},Nd^{3+} Sensitized $NaYF_4$ Core-Shell Nanocrystals on Ag Grating Film

Wen Xu,[a] Hongwei Song,[a] Xu Chen,[a] Haiyu Wang,[a] Shaobo Cui,[ab] Donglei Zhou,[a] Pingwei Zhou,[a] Sai Xu[a]*

Received (in XXX, XXX) Xth XXXXXXXXX 20XX, Accepted Xth XXXXXXXXX 20XX

DOI: 10.1039/b000000x

Here, we report the wavelength-dependent and angle-dependent upconversion luminescence (UCL) enhancement of $NaYF_4$:Yb^{3+},Tm^{3+}@$NaYF_4$:Yb^{3+},Nd^{3+} core-shell nanocrystals (NCs) resulting from Ag grating structure, which provides a novel insight of improving UCL.

In recent years, UCL of rare-earth (RE) doped fluoride nanomaterial has attracted extensive interests, because of their potential applications in solar cells and biological fluorescence imaging and detections.[1-5] Until now, Yb^{3+} sensitized UC nanomaterials such as $NaYF_4$:Yb^{3+},Er^{3+} has been commonly considered as the most efficient one under 980 nm excitation.[6] However, the smaller absorption cross-section of Yb^{3+} ions compared to organic dyes, quantum dots etc. and lower UCL efficiency has limited its practical applications. In previous works, many methods have been adopted to improve the UCL efficiency/strength, such as host selection, ions doping and core-shell design etc.[7-9] In recent years, surface plasmon enhanced UCL of emitters located in the metallic vicinity has been paid special attention, and the guiding principle for UCL enhancement is to tune the surface plasmon resonance (SPR) peak to the excitation/emission wavelength of the luminescent NCs.[10-13]

Surface plasmon polaritons (SPPs) are electromagnetic surface modes associated with collective electron oscillation propagating along the interface between a metal and a dielectric, which offers an effective way to improve electric field strength. In general, the excitation of SPPs is not possible on a smooth metallic surface because of the momentum mismatch between the wave vector of the SPPs and the incident light. Grating structure can overcome the momentum mismatch between the wave vector of SPPs and that of incident light.[14] And, the SPPs peak of grating can be easily adjusted to the excitation/emission wavelength through changing the sample angle, realizing the effective coupling.[15] However, the angle-dependent UC enhancement based on grating structure have not been reported yet.

In this work, we studied the angle-dependent effect of Ag grating structure on the UC enhancement of a novel $NaYF_4$:Yb^{3+}, Tm^{3+}@$NaYF_4$:Yb^{3+},Nd^{3+} core-shell NCs. Note that through the efficient energy transfer (ET) from Nd^{3+} to Yb^{3+} in the shell, the energy migration from shell Yb^{3+} to core Yb^{3+}, and the ET from Yb^{3+} to Tm^{3+} in the core, the excitation wavelength was successfully tuned from ~980 nm to ~800 nm, in which the tissue absorption can be largely suppressed and thus is more suitable for in vivo imaging and detection. [7,9] In this work, by varying the angle of excitation light, the UCL enhancement with several ten folds were obtained, under the excitation of both 808 nm and 980 nm laser diode.

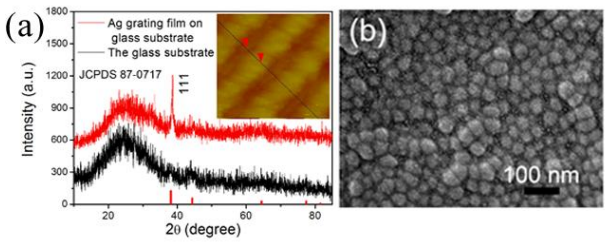

Fig.1 (a) the XRD patterns and AFM image (the inset) of the Ag grating on the glass substrate and the glass substrate. (b) the SEM image of Ag grating/$NaYF_4$:Yb^{3+},Tm^{3+} @$NaYF_4$:Yb^{3+},Nd^{3+} composite film.

First, the Ag grating and $NaYF_4$:Yb^{3+},Tm^{3+}@$NaYF_4$:Yb^{3+},Nd^{3+} core-shell NCs were prepared separately. Then, the solvent evaporation method was used to assemble the core-shell NCs layer-by-layer on the glass substrate and Ag grating. From XRD patterns of Fig.1 (a), the sharp diffraction peak of [111] face of Ag is clearly observed, and the broadband located at 15-30° originates from the glass substrate. We suggest that the Ag grating is pure cubic in phase and is with good crysrtallinity.[16] The inset shows the atomic force microscopy (AFM) image, indicating the formation of Ag grating structure. The detail analysis of Ag grating are shown in Fig.S1, and the grating periods and depth of Ag grating are determined, to be about 200 nm and 20 nm, respectively. Fig.1(b) shows the SEM image of Ag grating/$NaYF_4$:Yb^{3+},Tm^{3+} @$NaYF_4$:Yb^{3+},Nd^{3+} composite film, indicating that the dense layer with thickness of ~80 nm of $NaYF_4$:Yb,Er is formed on the Ag grating film. The $NaYF_4$:Yb^{3+},Tm^{3+}@ $NaYF_4$:Yb^{3+},Nd^{3+} nano-film has the same surface morphology and thickness with the composite film. The core-shell structure is examined carefully with TEM (See Fig.S2), the core and the shell thickness was determined to be 23 nm, 3.5 nm and 22 nm, 5 nm for $NaYF_4$:Yb^{3+},Tm^{3+}@$NaYF_4$:Yb^{3+},Nd^{3+} and $NaYF_4$:Yb^{3+},Nd^{3+} @$NaYF_4$:Yb^{3+},Tm^{3+} NCs, respectively.

The emission spectra of $NaYF_4$:Yb^{3+},Tm^{3+}@$NaYF_4$:Yb^{3+},Nd^{3+} and $NaYF_4$:Yb^{3+}, Nd^{3+} @$NaYF_4$:Yb^{3+}, Tm^{3+} core-shell NCs were shown in Fig.2, respectively. They exhibit intense

multiple emissions of Tm^{3+} ions spanning the UV-VIS regions under 980 nm and 808 nm excitation, assigned to the transitions of $^1I_6 \rightarrow {}^3F_4$ at 346 nm (five-photon populating), $^1D_2 \rightarrow {}^3H_6$ at 361 nm and $^1D_2 \rightarrow {}^3F_4$ at 451 nm (four-photon), $^1G_4 \rightarrow {}^3H_6$ at 475 nm and $^1G_4 \rightarrow {}^3F_4$ at 648 nm (three-photon), $^3F_2 \rightarrow {}^3H_6$ at 696 nm and $^3F_3 \rightarrow {}^3H_6$ at 726 nm (two-photon), respectively.[7,9] The overall UCL intensity of $NaYF_4:Yb^{3+},Tm^{3+}$ @$NaYF_4:Yb^{3+},Nd^{3+}$ (the luminescent centers Tm^{3+} locate in the inner sites) NCs is over 30 times than that of $NaYF_4:Yb^{3+},Nd^{3+}$ @$NaYF_4:Yb^{3+}$, Tm^{3+}(Tm^{3+} locate in the outer sites) NCs under the excitation of 200mW 980-nm light, and more, the relative intensity of high-order UCs in the former case increases considerably. This can be mainly attributed to the inhibition of nonradiative transition of Tm^{3+} after the shell forming, which departs the luminescent centers from large surface adsorption bonds.[17] In addition, as Nd^{3+} locates in the shell, the better thermal diffusion can decrease the local thermal effect.[7] The proposed ET path for Yb^{3+},Nd^{3+} sensitized UCL is shown in Fig2(b), as reported in previous literatures.[7,9] It is worth noting that under 808 nm excitation, the Nd^{3+} ions in the core are excited to $^4F_{5/2}$ state from the $^4I_{9/2}$ ground state, followed with nonradiative relaxation to the $^4F_{3/2}$ state. The energy would transfer to nearby Yb^{3+} and populate its $^2F_{5/2}$ state and further migrate to nearby Yb^{3+} ions crossing the shell. This energy migration route would initiate a typical UC process in the core, like as under 980 nm excitation.[18]

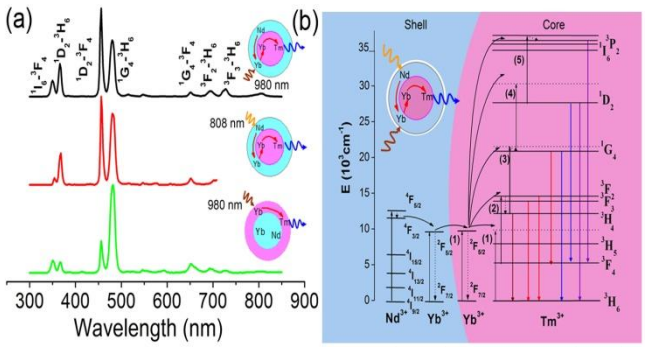

Fig.2 (a) the emission spectra of $NaYF_4:Yb^{3+},Tm^{3+}$ @$NaYF_4:Yb^{3+},Nd^{3+}$ and $NaYF_4:Yb^{3+}$, Nd^{3+}@$NaYF_4:Yb^{3+},Tm^{3+}$ core-shell NCs under 980 nm and 808 nm. (b) the proposed ET path for Yb^{3+},Nd^{3+} sensitized UC emissions.

Furthermore, we investigated the influence of Ag grating structure on UCL of $NaYF_4:Yb^{3+},Tm^{3+}$ @$NaYF_4:Yb^{3+},Nd^{3+}$ under 980 nm and 808 nm excitation. The sample structure and optical paths are as shown in Fig3(a) and (b). Fig.3 (c) shows the transmittance spectra of Ag grating/$NaYF_4:Yb^{3+},Tm^{3+}$ @$NaYF_4:Yb^{3+},Nd^{3+}$ composite film with varying the incident angle (0-60°). It can be seen that the SPPs split into two peaks and they shift toward opposite direction with increasing the incident angle. And they almost cover the wavelength region of 450-810 nm. The Ag grating has a low transmittance range of 400-1000nm owing to the Ag film absorption. Such unique transmission properties are the result of interaction between light and SPPs, which can be expressed as follows:[15]

$$K_{SPP} = K_0 \sin\theta \pm nK_g$$

where K_{spp} is the SPPs wave vector, $K_0\sin\theta = (2\pi/\lambda)\sin\theta$ is the in-plane wavevector of the incident photon, $K_g = 2\pi/G$ is the grating wavevector, G is the grating period, and n is an integer that defines the order of the scattering process. The dispersion relation was shown in Fig.3(d) by recording the peak wavelengths of SPPs as a function of angle θ. It is worth noting that as θ is at about 30°, 50°, 60°, the wavelength of SPP modes is consistent with the $^1D_2$-$^3F_4$/$^1G_4$-$^3H_6$, $^3F_2$,$^3F_3$-$^3H_6$ transitions, and the excitation at 808 nm, respectively. That is to say the SPPs mode of Ag grating can be easily adjusted to the excitation/emission wavelength through changing the sample angle and realize the effective coupling.

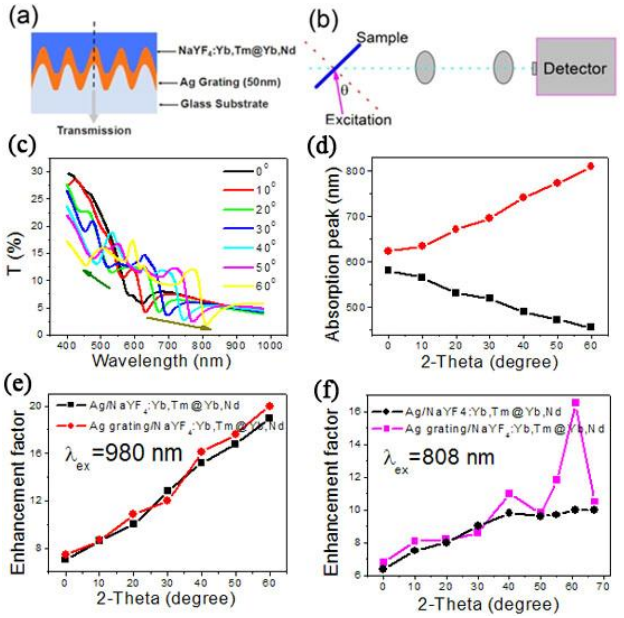

Fig.3 (a-b) the sample structure and optical paths for the transmittance and UCL spectra measurement. (c-d) the transmittance spectra and the related dispersion relation of Ag grating/$NaYF_4:Yb^{3+},Tm^{3+}$@$NaYF_4:Yb^{3+}$, Nd^{3+} composite film with varying the incident angle (θ). (e-f) the UCL enhancement factor as a function of incident angle (θ) under 980 nm and 808 nm excitation.

Fig.3(e) and 3(f) show the UCL enhancement factor under 980 nm and 808 nm excitation, respectively (EF, which is defined as the ratio of UCL intensity of the Ag grating/$NaYF_4:Yb^{3+},Tm^{3+}$ @$NaYF_4:Yb^{3+},Nd^{3+}$ composite film to that of $NaYF_4:Yb^{3+},Tm^{3+}$ @$NaYF_4:Yb^{3+},Nd^{3+}$ film (Ref) as a function of incident angle (θ). As a comparison, the EF in Ag/$NaYF_4:Yb^{3+},Tm^{3+}$@$NaYF_4:Yb^{3+},Nd^{3+}$ composite film (Ag with no grating structure) is also recorded. From Fig.3(e), it is observed that EF increases from 6-8 times to about 20 times as θ varying from 0° to 60° under 980 nm excitation, for both the traditional Ag film and Ag grating structure. This indicates that the variation of EF with the incident angle is related to the SPR of Ag nano-film, but has nothing to do with the grating structure.[16] Under 808 nm excitation (Fig.3f), the EF in Ag nano-film gradually increases from 7 to 10 times as θ increases from 0° to 70°. While in Ag grating structure, the EF increases from about 7 to 10 times as θ increases from 0° to 50°, which is similar to the result in Ag nano-film. When adjusts θ to 60°, the EF significantly improves to 17 fold, and as θ further increases to 70°, the EF decreases to about 11 times again. It can be concluded that as the θ is fixed at 60°, the SPPs peak locating at ~810nm matches well with the excitation wavelength, leading to the effective coupling between SSPs mode of Ag grating and the excitation light and a sudden increase of UCL. This is a direct evidence of the increase of excitation field in the Ag grating/UC NCs coupling system. It is suggested that under the 980 nm and

808 nm excitation, the emission coupling is not a main factor for the increase of UCL. This can be concluded by the similar EF for different transitions of Tm^{3+} in the composites (see Fig. S3). In order to further prove this point, the UCL dynamics are investigated under 980 nm and 808 nm excitation, respectively, and the results show that the decay time constants are almost same for the $NaYF_4$ sample on the glass reference and on the Ag grating (see Fig.S4), implying that the transition rate of Tm^{3+} on the Ag grating has little change. Thus the considerable UC enhancement can be mainly attributed to the coupling between the excitation light and the SPR of Ag film and SPPs mode of Ag grating.

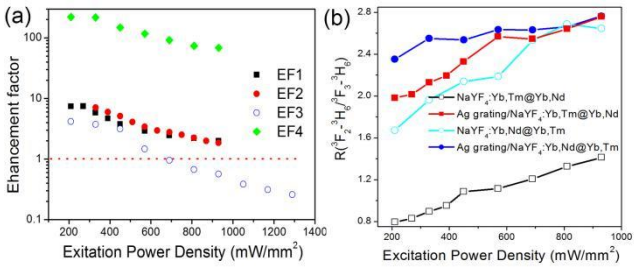

Fig.4 (a) EF1 and EF2 represent the UCL intensity ratio of the Ag grating/$NaYF_4$:Yb^{3+},Tm^{3+}@$NaYF_4$:Yb^{3+},Nd^{3+} composite film to $NaYF_4$:Yb^{3+},Tm^{3+} @$NaYF_4$:Yb^{3+},Nd^{3+} film under 980 nm and 808 nm excitation, respectively. EF3 represents the ratio of the Ag grating/$NaYF_4$:Yb^{3+}, Nd^{3+}@ $NaYF_4$:Yb^{3+},Tm^{3+}composite film to the $NaYF_4$:Yb^{3+}, Nd^{3+} @$NaYF_4$:Yb^{3+},Tm^{3+} film, EF4 represents the ratio of the Ag grating/$NaYF_4$:Yb^{3+},Tm^{3+} @$NaYF_4$: Yb^{3+},Nd^{3+} composite film to $NaYF_4$:Yb^{3+}, Nd^{3+} @$NaYF_4$:Yb^{3+},Tm^{3+} film under 980 nm. Fig.4(b), the intensity ratio (R) of $^3F_2$-$^3H_6$ to $^3F_3$-$^3H_6$ as a function of excitation power density in different samples.

In the Ag grating/$NaYF_4$:Yb^{3+},Tm^{3+} @$NaYF_4$:Yb^{3+},Nd^{3+} composite film, the UCL enhancement also depends strongly on excitation power density, and as a comparison, the Ag grating /$NaYF_4$:Yb^{3+},Nd^{3+} @$NaYF_4$:Yb^{3+},Tm^{3+} composite film were also investigated. Form Fig. 4(a), it can be seen that for all the samples, EF decreases with the increasing excitation power density, which can be attributed to the contribution of the saturation effect and/or the local thermal effect.[16] As the luminescent centers locate in the core, the decrease of EF (EF1 and EF2) with excitation power density is significantly slower than that of EF3 (the luminescent centers locate in the shell), which could be attributed to the suppressed thermal effect. In order to verify our hypothesis, the intensity ratio (R) of $^3F_2$-$^3H_6$ to $^3F_3$-$^3H_6$ is recorded as a function of excitation power in different samples in Fig.4 (b), which is a critical parameter to discuss the temperature change in UCL processes.[19] It can be clearly seen that under the same excitation power density the $NaYF_4$:Yb^{3+},Tm^{3+} @$NaYF_4$:Yb^{3+},Nd^{3+} nano-film has smaller R, implying the lower increase of local temperature increased by laser irradiation.[19] This shows that as the luminescent centers locate in the core, due to the existence of the passivation shell, the local thermal effect can be prevented to some extend, thus EF is over that as the luminescent centers locate in the shell. This can be further identified by the power-dependence of UCL in different samples (see Fig.S5). Finally, it is exciting to observe that as the excitation power density is lower, the UCL intensity of the Ag grating /$NaYF_4$:Yb^{3+},Tm^{3+}@$NaYF_4$: Yb^{3+},Nd^{3+} composite film is as high as ~200 times to that of $NaYF_4$:Yb^{3+},Nd^{3+}@ $NaYF_4$:Yb^{3+},Tm^{3+} film (EF4) under 980 nm excitation. From the results, we can know that in Ag grating/$NaYF_4$:Yb^{3+},Tm^{3+} @$NaYF_4$:Yb^{3+},Nd^{3+} composite film, the effective UCL enhancement and decreased thermal effect is realized by introducing the core-shell design and Ag grating structure. While, in the previous literatures,[10-13] the thermal effect has always been ignored.

In conclusion, the effect of Ag grating structure on the UCL enhancement of $NaYF_4$:Yb^{3+},Tm^{3+}@$NaYF_4$:Yb^{3+},Nd^{3+} core-shell NCs was studied. Several new points should be highlighted. First, in Ag grating/$NaYF_4$:Yb^{3+},Tm^{3+}@$NaYF_4$:Yb^{3+},Nd^{3+}nano-hybrids, the unique angle-dependent UCL enhancement was observed under 808 nm excitation. Second, it is interesting to observe that as the luminescence centers located in the core, the EF of UCL could be greatly improved due to the suppressed local thermal effect. Third, combining the core-shell design and the coupling of Ag grating, 200 folds UCL enhancement of Tm^{3+} was realized.

This work was supported by The Major State Basic Research Development Program of China (No. 2014CB643506), National Natural Science Foundation of China (Grant Nos. 11374127, 11304118, 61204015, 81201738, 61177042, 11174111, and 21273096).

Notes and references

[a]*State Key Laboratory on Integrated Optoelectronics, College of Electronic Science and Engineering, Jilin University, Changchun, 130012, People's Republic of China.*
[b]College of Physics, Jilin University, 2699 Qianjin Street, Changchun 130012, People's Republic of China.
E-mail: songhw@jlu.edu.cn

† Electronic Supplementary Information (ESI) available: [detail analysis of Ag grating film, TEM images of core-shell NCs, multicolor emission intensity profiles as a function of the excitation angle and power density, and UCL dynamics process].

1 (a) H. Q. Wang, M.Batentschuk, A. Osvet, L. Pinna and C. J. Brabec. Adv Mater., 2011, **23**, 2675-2680. (b) X. Y. Huang, S. Y. Han, W. Huang, X. G. Liu. Chem Soc Rev. 2013, **42**, 173-201.
2 F. Wang, R. R. Deng, X. G. Liu. Nature Protocols 2014, **9**, 1634-1644.
3 Y. S. Liu, D. T. Tu, X. Y. Chen. Chem Soc Rev. 2013, **42**, 6924-6958.
4 (a) S. L. Gai, C. X. Li, and J. Lin. Chem. Rev., 2014, **114**, 2343-2389. (b) C. X. Li and J. Lin. J. Mater. Chem., 2010, **20**, 6831–6847.
5 P. Huang, W. Zheng, S. Y. Zhou, D. T. Tu, Z. Chen, H. M. Zhu, R. F. Li, and X.Y. Chen, Angew. Chem. Int. Ed., 2014, **53**, 1252-1257.
6 F. Wang, and X. G. Liu, X. G. Chem. Soc. Rev. 2009, **38**, 976-98999.
7 Y. F. Wang, G.Y. Liu, L.D. Sun, J.W. Xiao, J. C Zhou, and C. H. Yan. ACS Nano., 2013, **7**, 7200-7206.
8 F. Wang and X. G. Liu. Acc. Chem. Res., 2014, **47**, 1378–1385.
9 X. J. Xie, N. Y. Gao, R. R. Deng, Q. Sun, Q. H. Xu, X. G. Liu. J. Am. Chem. Soc. 2013, **135**, 12608-12611.
10 N. Liu, W. P. Qin, G. S. Qin, T. Jiang, D. Zhao. Chem. Comm. 2011, **47**, 7671–7673.
11 H. Zhang, Y. J. Li, I. A. Ivanov, Y. Q. Qu, Y. Huang, and X. F. Duan. Angew. Chem. Int. Ed., 2010, **49**, 2865.
12 A. Priyam, N. M. Idris and Y. Zhang. J. Mater. Chem., 2012, **22**, 960.
13 F. Zhang, G. B. Braun, Y. F. Shi, Y. C. Zhang, X. H. Sun, N. O. Reich, D. Y. Zhao, and G. Stucky. J. Am. Chem. Soc., 2010, **132**, 2850.
14 Raether, H. Springer: Berlin/Heidelberg, 1988.
15 Y.Jiang, H. Y. Wang, H. Wang, B. R. Gao, Y. W. Hao, Y. Jin, Q. D. Chen, and H. B. Sun. J. Phys. Chem. C 2011, **115**, 12636–12642.
16 W. Xu, Y. S. Zhu, X. Chen, J. Wang, L. Tao, S. Xu, T. Liu, and H. W. Song. Nano Res.,2013, **6**, 795-807.
17 G. S. Yi and G. M. Chow . Chem. Mater. , 2007, **19**, 341–343.
18 V. Mahalingm, F. Vetrone, R. Naccache, A. Speghini, J. A. Capobianco. Adv. Mater., 2009, **21**, 4025.
19 B. Dong, H. W. Song, H. Q. Yu, H. Zhang, R. F. Qin, X. Bai, G. H. Pan, S. Z. Lu, F. Wang. J. Phys. Chem. C 2008, **112**, 1435-1440.